Microscopic Insights into the Sputtering of Thin Organic Films on Ag{111} Induced by C_{60} and Ga Bombardment

Zbigniew Postawa,*,† Bartlomiej Czerwinski,† Nicholas Winograd,‡ and Barbara J. Garrison*,‡

Smoluchowski Institute of Physics, Jagiellonian University, Krakow, Poland, and Department of Chemistry, 104 Chemistry Building, The Pennsylvania State University, University Park, Pennsylvania 16802

Received: February 16, 2005; In Final Form: April 25, 2005

This paper contains enhanced objects available on the Internet at http://pubs.acs.org/jpcbfk.

Molecular dynamics computer simulations have been employed to model the bombardment of Ag{111} covered with three layers of C_6H_6 by 15 keV Ga and C_{60} projectiles. The study is aimed toward examining the mechanism by which molecules are desorbed from surfaces by energetic cluster ion beams and toward elucidating the differences between cluster bombardment and atom bombardment. The results show that the impact of the cluster on the benzene-covered surface leads to molecular desorption during the formation of a mesoscopic scale impact crater via a catapulting mechanism. Because of the high yield of C_6H_6 with both Ga and C_{60}, the yield enhancement is observed to be consistent with related experimental observations. Specific energy and angle distributions are shown to be associated with the catapult mechanism.

1. Introduction

Cluster ion beams are recognized as valuable sources for desorption of high mass ions in time-of-flight secondary ion mass spectrometry (TOF−SIMS) experiments as highlighted in a recent article in *Nature*[1] and in an overview article in *Analytical Chemistry*.[2] Their use received a boost about 5 years ago when an SF_5^+ ion source was introduced commercially.[3,4] There have recently been reports of two additional cluster beam sources consisting of gold trimer,[5,6] Au_3^+, and buckyball,[7,8] C_{60}^+, ion beams that overcome lateral resolution and lifetime issues associated with the SF_5^+ gun. Results from experiments utilizing these ion sources are quite promising.[2] For instance, the yield of the peptide gramicidin is enhanced by a factor of 1300 during C_{60} impact when compared to Ga^+ ion bombardment.[7] Moreover, there is growing evidence that the C_{60}^+ ion beam can be utilized in molecular depth profiling experiments.[9−14]

The reasons behind the unique properties of cluster ion beams are still not well-understood. Various degrees of enhancement of high mass secondary ions have been reported, depending upon the type of projectile, target material, and matrix.[3] For example, thin polymer films on Ag do not seem to benefit from the use of polyatomic projectiles, while SIMS spectra from bulk polymers are dramatically improved.[3] Theoretical calculations are beginning to unravel some of the phenomena responsible for cluster-induced sample erosion.[15−22] Molecular dynamics (MD) simulations of C_{60} impact with kinetic energies in the range of 10−20 keV on graphite[19,23] and diamond[20] show that a crater forms and that the energy is deposited in the near surface region. Calculations of small metal cluster bombardment in the same energy range predict similar crater formation on graphite and metal substrates.[15,17,22,24] At lower kinetic energies, it has been shown that the mass of the substrate is important in determining the mechanism of the enhancement effect.[21] For the case of benzene adsorbed on a graphite surface, it has been shown that C_{60} bombardment gives rise to an acoustic wave that lifts off the molecules.[25]

To understand the signal enhancement in TOF−SIMS experiments and to predict optimal experimental configurations, we have initiated a comprehensive series of MD investigations aimed toward understanding collision cascades due to keV C_{60} cluster bombardment.[26−28] The strategy involves utilizing well-defined model substrates to elucidate how the atomic motion and subsequent measurable quantities depend on the nature of the incident particle, either an atomic species such as Ga or the cluster C_{60}. Here, we focus on the study of C_6H_6 overlayers on the Ag{111} surface to establish the special motion, if any, that cluster bombardment provides in enhancing the desorption of weakly bound molecular species. Although this simple system does not include effects such as strong binding to the surface or molecular entanglement of large molecules, it does provide a good model for understanding the role of the substrate metal in the desorption process. Moreover, we have already reported on both experimental and MD simulations for this system using ion bombardment.[29] The close agreement of the kinetic energy and angle distributions of sputtered C_6H_6 molecules gives us confidence to proceed to the cluster bombardment regime.

The results show that crater formation observed on the clean Ag{111} surface is retained during bombardment of molecular overlayers. In fact, the formation of the crater itself is intimately involved in the desorption mechanism through a catapult-like mechanism and is reflected in both kinetic energy and angle distributions. Moreover, comparison of collision cascades for atomic and cluster bombardment on these thin film systems suggest that yield enhancements are not particularly large, a result also observed by experiment.

2. Model Details

Molecular dynamics (MD) computer simulations have successfully described the dynamics due to cluster bombardment

* Corresponding authors. E-mail: zp@castor.if.uj.edu.pl; Phone: (4812) 632-4888 ext. 5626. E-mail: bjg@psu.edu; Phone: (814) 863-2103.

† Jagiellonian University.

‡ The Pennsylvania State University.

10.1021/jp050821w CCC: $30.25
Published on Web 05/25/2005

on metal, graphite, and diamond surfaces, as mentioned above. In addition, these simulations have been employed to model the ejection of molecules from benzene overlayers on metal substrates where there are direct comparisons to experimental data of energy and angular distributions.[30] Thus the MD method is utilized to elucidate the differences between Ga and C_{60} bombardment of three layers of benzene on Ag{111}. Briefly, the motion of the particles is determined by integrating Hamilton's equations of motion.[31−33] The forces among the atoms are described by a blend of empirical pairwise additive and many-body potential energy functions. The Ag−Ag interactions are described by the molecular dynamics/Monte Carlo corrected effective medium (MD/MC−CEM) potential for fcc metals.[34] The Ga−Ag, Ga−C, and Ga−H interactions are described using the purely repulsive Molière pairwise additive potential. The adaptive intermolecular potential, AIREBO, developed by Stuart and co-workers is used to describe the hydrocarbon interactions.[35] This potential is based on the reactive empirical bond-order (REBO) potential developed by Brenner for hydrocarbon molecules.[36−38] The AIREBO potential yields a binding energy per atom in the relaxed C_{60} cluster of 7.2 eV, which compares well with the experimental value of 7.4 eV.[35] Finally, the interaction of C and H atoms with Ag atoms is described by a Lennard-Jones potential using established parameters.[28]

The model approximating the Ag{111} substrate consists of a finite microcrystallite containing 166 530 atoms arranged in 39 layers of 4270 atoms each.[26,27] The sample size ($175 \times 174.5 \times 89.7$ Å) was chosen to minimize edge effects associated with the dynamical events leading to ejection of particles. Organic overlayers are represented by three layers of C_6H_6 molecules deposited on the surface of the Ag crystal. More information about the model and other details of simulations can be found elsewhere.[26] Projectiles of 15 keV Ga and C_{60} are directed normal to the surface. A total of 23 trajectories were calculated for 15 keV Ga, and 16 trajectories were sampled for 15 keV C_{60}. As discussed previously,[26] the motion induced by C_{60} bombardment is mostly independent of the initial aiming point. For Ga bombardment of the benzene overlayer, there is also less dependence on the impact point than for Ga bombardment of the clean Ag surface. For instance, the standard deviation of the total sputtering yield is comparable for clean (see Table 2 of ref 26) and benzene-covered silver crystal, whereas 300 and barely 23 trajectories were sampled, respectively. Consequently, only a few impact points need to be sampled to obtain reliable statistics. Each trajectory was initiated with a fresh sample with all atoms in their equilibrium minimum energy positions. The atoms in the target initially have zero velocity. The atoms in the C_{60} projectile initially have no velocity relative to the center of mass motion. The trajectory is terminated when the total energy of the most energetic particle remaining in the solid is less than 0.05 eV. In our case, the binding energy of Ag is 2.95 eV and the binding energy of the benzene overlayer is approximately 0.4 eV. The time of each trajectory ranges between 9 and 15 ps and depends on the type of primary projectile, its impact point, and the manner in which the energy distributes within the solid.

There are two aspects of the computational setup that require special care. First, large pressure waves[16,17,22−24,39] are generated by the C_{60} bombardment that could possibly cause artifacts if allowed to reflect from the boundaries of the sample. Briefly, for the boundary conditions, a stochastic region[40,41] at 0 K and a rigid layer are put on five sides of the crystal. Second, the definition of ejected species must be carefully examined due to the eruption of the material caused by the C_{60} impact as shown in Figure 1. The implementation of the approaches to overcome these limitations has been previously described.[26,27]

The final computation issue to address is the stability of ejected clusters. The clusters at end of trajectory after ~15 ps may have sufficient energy to dissociate before reaching a detector tens of microseconds later. It has been shown that there is a direct correlation between the internal and kinetic energy of ejected molecules.[29] Therefore, more energetic molecules have on average more internal energy and, consequently, they will be more prone to dissociate on the way to the detector.[29,42−44] One strategy for taking this phenomenon into account is to integrate their equations of motion for a sufficiently long time such that the likelihood of further dissociation is small.[42] This strategy is successful when the interaction potential is reliable for dissociation channels and when the decay time is less than a time of 10^{-9} s. The application of this approach to bombardment of a clean metal showed that there were changes to the cluster and monomer yields and energy distributions between the time a few ps after the bombardment event and several hundred ps later.[42,43]

An alternative strategy is to use a fixed cutoff value of the internal energy to determine which molecules will dissociate.[29,44] This approach for different size molecules is described in detail elsewhere.[44] This strategy is best when the interaction potential is not sufficient for describing the dissociation pathways, as is the case here for the hydrocarbon species. The downside to this approach is that the effect of the dissociation events on the smaller decay products is not included.

For the simulations here, a constant value of internal energy is used to estimate whether a C_6H_6 molecule will dissociate. The prescription for defining the internal energy was given previously.[44] It is known from experiments that the most probable channel of C_6H_6 decay is loss of a H atom.[45,46] Unimolecular decomposition theory predicts that more than 90% of C_6H_6 molecules will be detected on a μs time scale[44] if their internal energy does not exceed 4.6 eV. Therefore, this value is used as a dissociation threshold.

The dissociation of van der Waals complexes, such as $(C_6H_6)_n$, is even harder to estimate. The classical simulations will not correctly describe the energy flow from the high frequency intramolecular vibrational modes into the low frequency intermolecular motions. Consequently we exercise caution in interpreting the quantitative data regarding these clusters.

3. Results and Discussion

The discussion starts with an overview of the basic collision events for Ga and C_{60} bombardment as the mechanisms provide the foundation for understanding the other properties. The ejection yields are discussed next, followed by the internal energy, kinetic, and angular distributions.

Mechanisms. Snapshots of the temporal evolution of typical collision events leading to ejection of particles due to 15 keV Ga and C_{60} bombardment are shown in Figure 1 and Figure 2. Animations of the same events are shown in as web-enhanced objects. A significant portion of the benzene overlayer is altered upon the impact of either projectile. The nature of the collision events leading to these changes, however, is different for Ga and C_{60}. The Ga projectile easily penetrates through the organic overlayer losing, on average, only ~0.4 keV of the initial 15 keV. Direct collisions between Ga and benzene molecules lead to the formation of energetic organic fragments. The majority

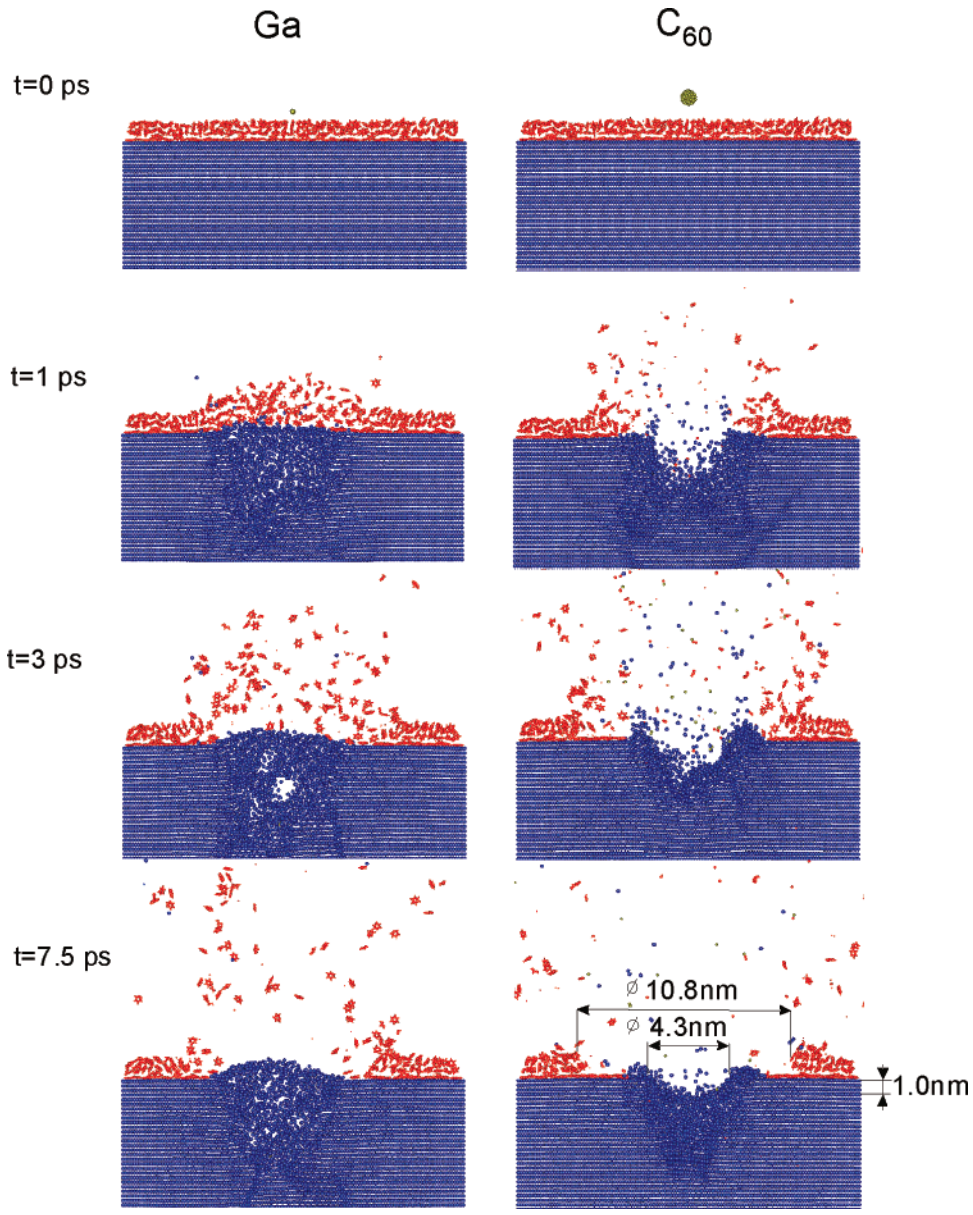

Figure 1. Cross sectional view of the temporal evolution of a typical collision event leading to ejection of particles due to 15 keV Ga and C_{60} bombardment at normal incidence of a three layer benzene system deposited upon a Ag{111} surface. The dimensions on the 7.5 ps snapshot of the C_{60} bombardment is for the depth and width of the Ag crater and the swept-out region of the benzene overlayer. A slice 1.5 nm wide in the center of the system is shown.

Ⓦ Video animations in .avi format showing Ⓦ Ga bombardment and Ⓦ C_{60} bombardment are available.

of these fragments move through the overlayer toward the Ag surface, and in the process create more fragments. After reaching the Ag surface, the fragments are predominantly reflected back into the organic overlayer. During this stage of the motion, predominantly fragments are created. As the cascade progresses, collisions between moving particles and intact C_6H_6 molecules become less energetic and more molecules are set into motion. The calculations indicate that approximately 20% of all ejected C_6H_6 molecules due to Ga bombardment are formed by processes initiated in the overlayer.

After passing through the organic overlayer, the Ga projectile penetrates into the substrate, depositing most of its kinetic energy at a considerable depth similar to the motion induced without the overlayer.[26,27] The energy is subsequently redistributed within the crystal and a highly excited cylindrical volume is formed. Only a small portion of the primary energy is deposited near the Ag surface leading to ejection of substrate particles. These upward moving Ag particles collide with the C_6H_6 molecules located above them, leading to ejection of molecules and fragments in a manner similar to that observed in previous simulations of 0.5−5 keV Ar bombardment.[29,31,32,44,47−51] Ejection of Ag atoms induced by 15 keV Ga occurs in a relatively short time. For instance, most of ejection events occur within 1.7 ps for the clean Ag system.[26,27] Collisions between upward moving Ag particles and organic molecules initiate the process of molecular ejection as seen in Figure 1 in the 1 ps frame. The kinetic energy of ejecting Ag atoms is low and integrity of the organic overlayer is preserved during this period. Almost no Ag particles are emitted into the vacuum. Even after 1.7 ps, however, there is still considerable disruption in the substrate as evidenced by the cavity apparent in the 3 ps snapshot in Figure 1. Due to the subsurface collision cascade, there is a correlated upward motion of Ag atoms toward the surface. There is sufficient kinetic energy to eject the remaining portion of the loosely bound benzene overlayer as shown in the 3 ps frame. The process continues up to approximately 8 ps and then the

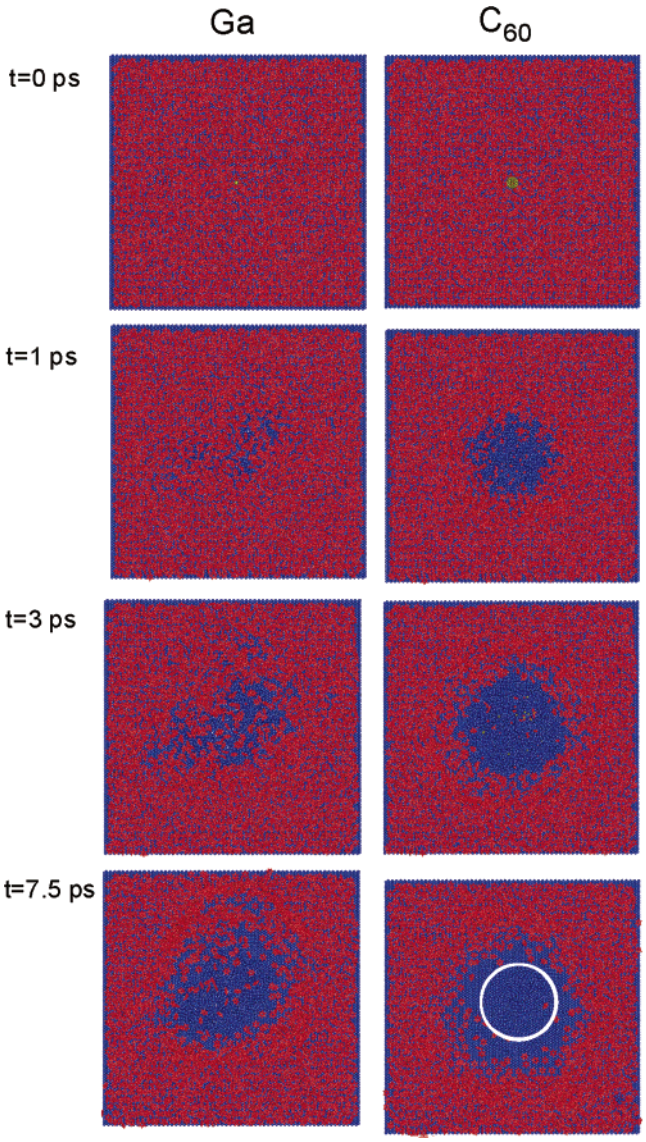

Figure 2. Top view of the temporal evolution of the collision sequences shown in Figure 1. The white circle denotes the outer rim of the crater formed in the Ag substrate by C_{60} impact.

ejection ceases. The final configuration has most of the C_6H_6 molecules in the region where the Ga particle struck the surface removed.

A different scenario takes place during C_{60} impact as shown in Figure 1 and Figure 2. Due to its much larger size, C_{60} interacts strongly with the benzene overlayer. Although the integrity of the projectile is lost almost immediately upon impact, the C atoms continue their downward motion. On average, 8.8 keV of the initial kinetic energy is deposited into the benzene overlayer by the 15 keV C_{60} projectile. This increased efficiency of the energy deposition is a consequence of the larger collision cross section with the benzene overlayer. Each C atom collides with the surface, with only 250 eV of initial kinetic energy rather than the 15 keV associated with the Ga projectile.

After impact on the Ag substrate, the spatial correlation of C atom movements is lost. Due to the heavier mass of the substrate Ag atoms, most of the C atoms originating from the projectile are reflected toward the organic overlayer. Consequently, the energy of the cluster projectile is deposited in a shallow volume of the substrate in a short time, leading to the ejection of many substrate particles. Similar to the dynamics for a clean Ag substrate, a crater is formed.[26,27] The process is almost mesoscopic in character and only weakly depends on the initial impact point of the C_{60} molecule on the surface. Since a significant portion of the primary kinetic energy is dissipated during penetration of the organic overlayer, the size of the crater, diameter of 4.3 nm and depth of 1 nm, is significantly smaller than the crater for clean Ag{111}, diameter of 5.4 nm and a depth of 1.8 nm.[27] This crater formation leads to a temporally and spatially correlated motion of metal substrate particles as shown in Figure 1 at about 3 ps. The average kinetic energy of atoms taking part in this process is larger than for atoms involved in the formation of the bulge during Ga bombardment. These particles collectively interact with adsorbed C_6H_6 molecules, uplifting most of the remaining molecules in this area. As seen in Figure 1 at 3 ps the molecules are removed much earlier than for Ga bombardment. The final altered area, however, is comparable in both cases and has a diameter of approximately 11 nm.

TABLE 1: Number of Particles Ejected from Three Layer C_6H_6/Ag{111} System Bombarded by 15 KeV Ga and C_{60} Projectiles at normal Incidence at 15 ps after the Ion Impact[a]

projectile particle	Ga	C_{60}	enhancement
total Ag yield	15 ± 3	81 ± 6	5.4
total C_6H_6 yield	227 ± 33	400 ± 8	1.8
C_6H_6 molecules	120 ± 18	244 ± 3	2.0
C_6H_6 equivalents in smaller clusters and fragments	8.5 ± 3	82 ± 4	9.6
C_6H_6 molecules in larger clusters	99 ± 22	75 ± 5	0.8

[a] The total yields for Ag and C_6H_6 are irrespective of the chemical species ejected. The enhancement is the ratio of the C_{60} yield to the Ga yield. The errors represent the standard deviations of our data.

Although direct interactions between C_{60} and the organic overlayer predominantly lead to creation of numerous energetic fragments, the C_{60} penetration of the overlayer initiates another process. An almost planar pressure wave is generated that propagates in the organic overlayer parallel to C_6H_6/Ag interface. The propagation of the pressure wave does not contribute significantly to molecular ejection but mainly relocates C_6H_6 molecules away from the impact point of the C_{60} projectile. As a result, a circular rim (Figure 1, 7.5 ps) is formed from piled-up C_6H_6 molecules, and the altered volume of the organic overlayer extends far beyond the area of the crater formed in the substrate material. This effect is facilitated by the weak binding of the C_6H_6 to the metal substrate and the weak binding within the overlayer.

Yields. The sputtering or ejection yields are given in Table 1 and the mass distribution at 15 ps is shown in Figure 3. Emission of intact C_6H_6 molecules is the main result of Ga bombardment, whereas a significant number of substrate particles and small hydrocarbon fragments eject due to the C_{60} bombardment. The number of ejected C_6H_6 molecules is larger for the C_{60} projectile than for the Ga projectile. The enhancement of 1.8, however, is significantly smaller than the enhancement of 5.4 observed in the sputtering yield of substrate Ag particles. In fact, a 15-fold enhancement has been reported for 15 keV C_{60} and Ga projectiles bombarding clean Ag{111} surface at normal incidence.[26,27] At first, this may seem to be a bit unexpected since MD studies of the sputtering of organic monolayers show that molecules are emitted mainly due to collisions with departing substrate atoms.[29,32,50,51] Several factors, however, are responsible for the smaller enhancement factor. First, there is a limited number of physisorbed C_6H_6 molecules available for desorption and the binding energy of the overlayer is low (0.4 eV). Consequently, most of the adsorbed C_6H_6

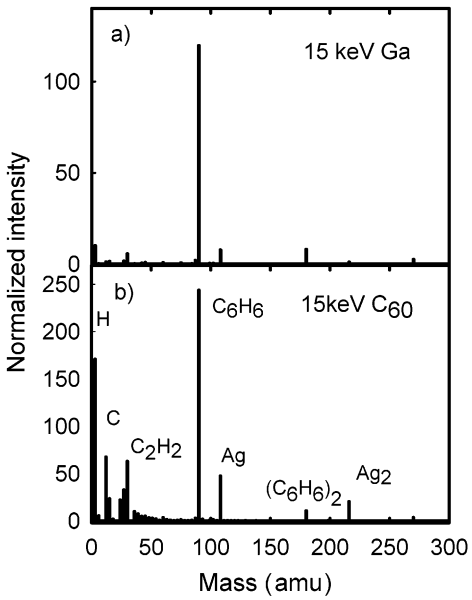

Figure 3. Mass distribution up to 300 amu of particles ejected by 15 keV Ga and 15 keV C_{60} bombardment collected ~15 ps after the projectile impact.

molecules are emitted even by the less energetic processes initiated by the Ga impact as shown in Figure 2. Second, the impact of the C_{60} projectile generates a pressure wave that propagates in the organic overlayer pushing the molecules away from the point of impact. As a result, many of the substrate particles ejecting during C_{60} bombardment do not have a chance to collide with C_6H_6 molecules. Finally, as shown in Figure 3 and Table 1, significant fragmentation of C_6H_6 molecules occurs due to the C_{60} impact, which additionally reduces the probability of intact molecule ejection.

The final observation regarding the yields is the relatively large number of C_6H_6 molecules for both projectiles aggregated in larger clusters such as $(C_6H_6)_n$, with n ranging from 2 to over 100. It is probable that these weakly bound clusters will dissociate during the tens of microseconds flight path to the detector. Since the larger clusters will dissociate, no significance is attached at this time to the larger cluster yield for Ga bombardment.

Internal Energy and Dissociation. The yields given in Table 1 and Figure 3 identify all particles that are ejected from the surface at 15 ps after the projectile impact. To evaluate the role of unimolecular dissociation, the internal energy distributions of C_6H_6 molecules collected at 15 ps after the projectile impact are given in Figure 4. Most of the C_6H_6 molecules ejected by Ga have an internal energy lower than the assumed dissociation threshold of 4.6 eV. On the other hand, ~21% of molecules ejected by C_{60} impact have internal energies exceeding the threshold value. All of these molecules will dissociate and, consequently, they will not be detected. As seen in Figure 1, the larger internal excitation can be explained by taking into account the more violent processes that follow the C_{60} impact. Because of the decrease in benzene yield with the C_{60} projectile due to dissociation, the enhancement factor is reduced from 1.8 to 1.4.

Kinetic Energy Distributions. The kinetic energy distribution of ejected particles is a quantity that can be measured and, at times, can be used to help understand the mechanisms responsible for emission. Angle integrated kinetic energy distributions of C_6H_6 molecules ejected due to 15 keV Ga and C_{60} projectiles are displayed in Figure 5. Solid (C_{60}) and dashed

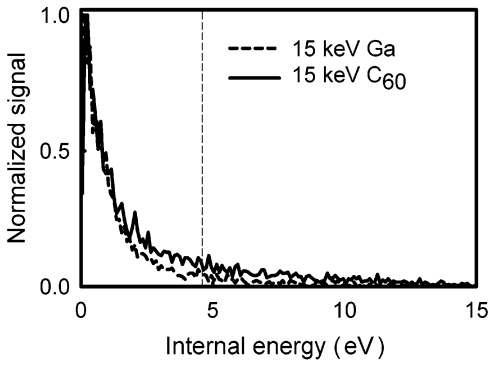

Figure 4. Internal energy distribution of C_6H_6 molecules ejected by 15 keV Ga (dashed line) and 15 keV C_{60} (solid line) bombardment. The vertical dashed line is the cutoff energy used to determine which molecules will unimolecularly decay during the tens of microseconds flight time to the detector.

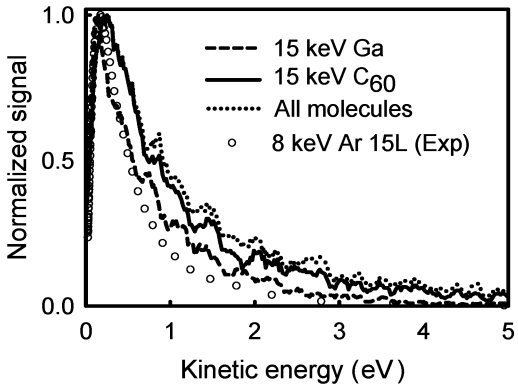

Figure 5. Peak normalized kinetic energy distributions of C_6H_6 molecules sputtered at normal incidence from Ag{111} by 15 keV Ga and C_{60}. Solid and dashed lines depict molecules ejected with internal energy less than 4.6 eV. Dotted and dash dotted lines indicate all ejected C_6H_6 molecules, while circles depict experimental data obtained from 8 keV Ar bombardment of a benzene overlayer formed from a 15 Langmuir exposure of Ag{111} surface at 100 K.

(Ga) lines depict the kinetic energy distributions of molecules with the internal energy lower than the assumed dissociation threshold. The dotted lines depict uncorrected spectra for C_{60} collected at 15 ps. Eliminating the molecules with more than 4.6 eV of internal energy preferentially affects the higher kinetic energy portion of the distribution, as was found for atomic bombardment.[29] The effect is noticeable for C_{60} and negligible for Ga. The kinetic energy distributions are consistent with the picture in which more energetic processes are involved in ejection of C_6H_6 molecules due to C_{60} bombardment vs Ga bombardment. Since no experimental data yet exist for Ga and C_{60} bombardment of a benzene overlayer, the kinetic energy spectrum obtained for 8 keV Ar bombardment of a benzene multilayer[52] is shown in Figure 5. The agreement between the calculated and measured kinetic energy distributions is respectable, taking into account difference in the projectile's kinetic energy and type of projectile.

Angular Distributions. The dependences of the desorption yields of selected organic species on their initial positions relative to the projectile point of impact are given in Figure 6. For Ga bombardment the distributions are not particularly informative. The hydrocarbon fragments and C_6H_6 molecules originate from a region centered at the impact point with the fragments originating from a smaller region. The origin of the C_6H_6 dimers is scattered. In contrast, the distributions depicting the origin of emitted C_6H_6 molecules provide a graphical

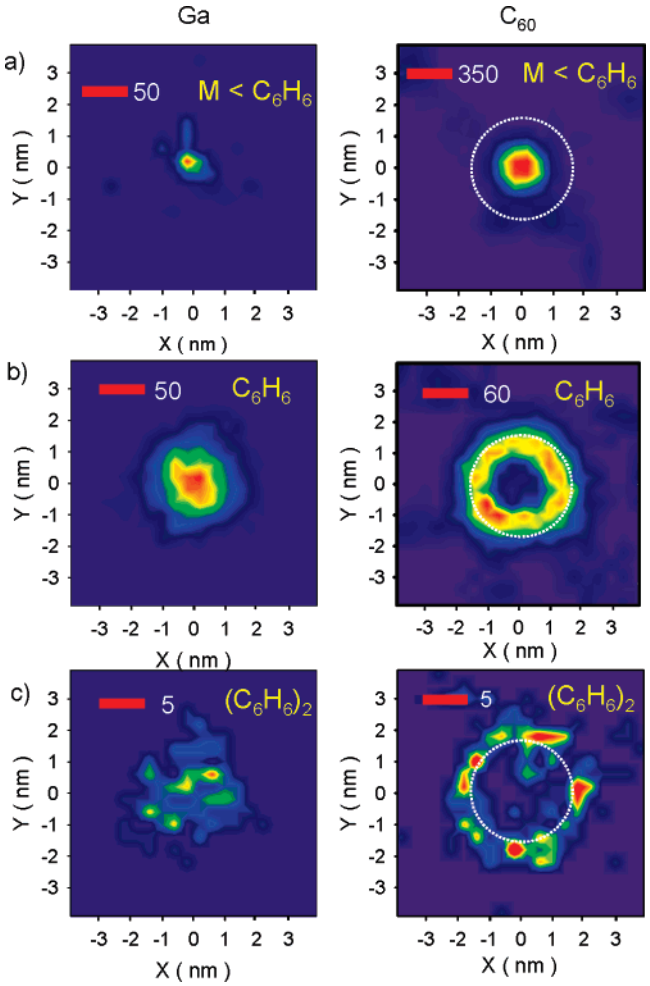

Figure 6. Spatial distribution of original location of (a) molecular fragments, (b) C_6H_6 molecules, and (c) dibenzene complexes sputtered by 15 keV Ga and 15 keV C_{60} bombardment at normal incidence. The red bars indicate the highest intensity in each frame. The white dashed circle for the C_{60} plots corresponds to a diameter of 4.3 nm.

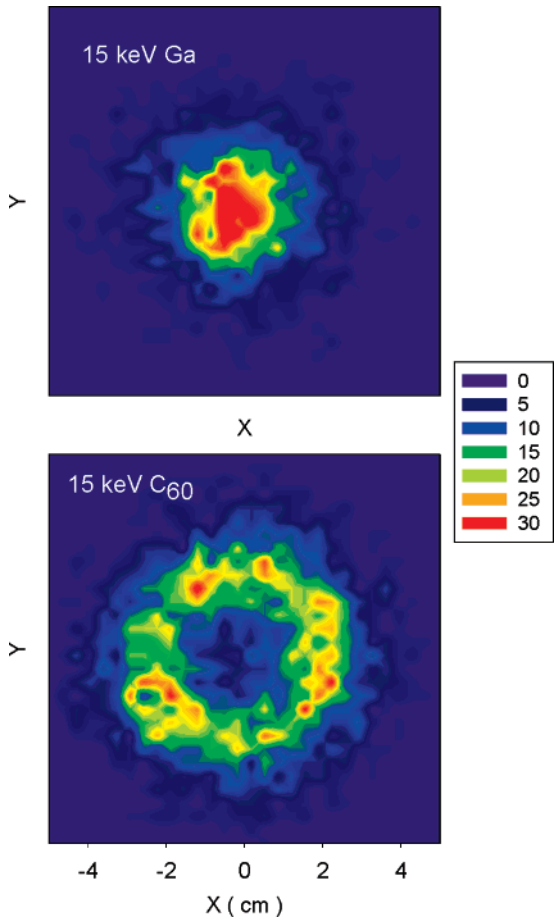

Figure 7. Angular distribution of C_6H_6 molecules ejected by 15 keV Ga (top) and 15 keV C_{60} (bottom) bombardment at normal incidence. The data are presented for deposition on a flat plate collector located 3 cm in front of the surface. The peak in the angular distribution for the C_{60} bombardment is at about 40° from the surface normal.

illustration of the various mechanisms involved in the C_{60} bombardment event as delineated below.

(i) Molecular fragments are formed by direct interaction of the C_{60} particle with the benzene overlayer. As mentioned above, the C_{60} is fragmented just after impact and then the separate C atoms with high kinetic energy move through the organic overlayer, fragmenting molecules. As shown in Figure 6, the extent of the induced damage is limited to 1.6 nm, an area slightly larger than the diameter of the C_{60} cluster (0.7 nm).

(ii) As visible in the animations of our simulations, intact molecules are ejected by a concerted action of Ag atoms involved in the unfolding of the crater. The motion of these atoms is spatially and temporally correlated, and they have a relatively low kinetic energy (<3 eV). The upheaval of the crater rim gives the momentum to the molecules. The unfolding of the crater acts, therefore, as a sling or catapult that hurls the organic molecules into the vacuum. The intact C_6H_6 molecules originate from a ring-like region close to the inside of the final rim of a crater, diameter of 4.3 nm, formed in the substrate. This ejection mechanism should have a visible effect on the angular characteristics of molecular emission. Indeed, as presented in Figure 7, ejection of C_6H_6 exhibits a distinct ring-like structure that mimics the geometry of the underlying crater. The ejection is azimuthally isotropic and peaks at a polar angle of approximately 40° with respect to the surface normal. The azimuthal isotropy is also observed in the angular distribution of molecules ejected by Ga impact as shown in Figure 7 but, in this case, the emission peaks along the normal to the surface.

(iii) Dibenzene complexes are formed at the final stage of the unfolding of the crater. As depicted at 3 ps in Figure 1, the opening of the crater correlates the upward motion of C_6H_6 molecules, increasing the probability of van der Waals complex formation. Dibenzene complexes are also formed during the overlayer compression induced by an upward distortion of the altered substrate region due to Ga impact. Their original positions, however, do not reflect any special motion. Since the ejection of the benzene complexes results from strongly correlated motions in both cases, it is not surprising that the size of the initial clusters extends to as many as 100 benzene molecules.

4. Conclusions and Implications

The observations presented in this paper provide insight into the efficacy of C_{60} cluster beams for molecular desorption in TOF−SIMS experiments. Although enhancements of greater than 300-fold have been observed for peptide molecules with molecular weights of up to several thousand Daltons,[7,8] comparable enhancements are not observed for thin organic layers on inorganic substrates.[7,11] These simulations corroborate this finding and attribute the lack of improvement to a limited number of weakly bound molecules available for desorption. Essentially, both the Ga and C_{60} particles remove most of the material in the region of impact, although the mechanisms responsible for material removal are different.

The data presented in this paper relate to the sputtering of neutral organic molecules. The experimental data on the other hand generally consist of the mass spectra for ionic species. The specific ionization and neutralization mechanisms that are operative for atomic and polyatomic bombardment are still not understood. Predictions such as emission enhancement, creation of the crater, possibility to achieve better depth resolution are applicable to the study of both ions and neutrals. By no means, however, should quantitative comparisons between emission enhancements of ions be inferred from this study. For such analysis, ionization and neutralization processes should be included into the model calculations. This is still an unresolved problem, although, some promising attempts are already being made.[53−55]

Acknowledgment. The financial support from the Polish Committee for Scientific Research program no. 3T09A12426, CYFRONET and National Science Foundation are gratefully acknowledged. The Academic Services and Emerging Technologies group at Penn State provided us early access to the lion-xl PC cluster.

References and Notes

(1) Castner, D. G. *Nature* **2003**, *422*, 129.
(2) Winograd, N. *Anal. Chem.* **2005**, *77*, 142A.
(3) Kotter, F.; Benninghoven, A. *Appl. Surf. Sci.* **1998**, *133*, 47.
(4) Gillen, G.; Walker, M.; Thompson, P.; Bennett, J. *J. Vac. Sci. Technol. B* **2000**, *18*, 503.
(5) Davies, N.; Weibel, D. E.; Blenkinsopp, P.; Lockyer, N.; Hill, R.; Vickerman, J. C. *Appl. Surf. Sci.* **2003**, *203*, 223.
(6) Kersting, R. P.; Hagenhoff, B.; Verlaek, R.; Stapel, D.; Benninghoven, A.; Schwede, B. C. *Proceedings of the International Conference on Secondary Ion Mass Spectrometry*, 12th, Brussels, Belgium, Sept. 5−10 **2000**, 825.
(7) Weibel, D.; Wong, S.; Lockyer, N.; Blenkinsopp, P.; Hill, R.; Vickerman, J. C. *Anal. Chem.* **2003**, *75*, 1754.
(8) Wong, S. C. C.; Hill, R.; Blenkinsopp, P.; Lockyer, N. P.; Weibel, D. E.; Vickerman, J. C. *Appl. Surf. Sci.* **2003**, *203*, 219.
(9) Sun, S.; Szakal, C.; Roll, T.; Mazarov, P.; Wucher, A.; Winograd, N. *Surf. Interface Anal.* **2004**, *36*, 1367.
(10) Szakal, C.; Sun, S.; Wucher, A.; Winograd, N. *Appl. Surf. Sci.* **2004**, *231−2*, 183.
(11) Sostarecz, A. G.; Sun, S.; Szakal, C.; Wucher, A.; Winograd, N. *Appl. Surf. Sci.* **2004**, *231−2*, 179.
(12) Sun, S.; Wucher, A.; Szakal, C.; Winograd, N. *Appl. Phys. Lett.* **2004**, *84*, 5177.
(13) Wucher, A.; Sun, S.; Szakal, C.; Winograd, N. *Appl. Surf. Sci.* **2004**, *231−2*, 68.
(14) Wucher, A.; Sun, S. X.; Szakal, C.; Winograd, N. *Anal. Chem.* **2004**, *76*, 7234.
(15) Webb, R.; Kerford, M.; Way, A.; Wilson, I. *Nucl. Instrum. Methods Phys. Res., Sect. B* **1999**, *153*, 284.
(16) Colla, T. J.; Aderjan, R.; Kissel, R.; Urbassek, H. M. *Phys. Rev. B* **2000**, *62*, 8487.
(17) Aderjan, R.; Urbassek, H. M. *Nucl. Instrum. Methods Phys. Res., Sect. B* **2000**, *164*, 697.
(18) Kerford, M.; Webb, R. P. *Nucl. Instrum. Methods Phys. Res., Sect. B* **1999**, *153*, 270.
(19) Seki, T.; Aoki, T.; Tanomura, M.; Matsuo, J.; Yamada, I. *Mater. Chem. Phys.* **1998**, *54*, 143.
(20) Aoki, T.; Seki, T.; Matsuo, J.; Insepov, Z.; Yamada, I. *Mater. Chem. Phys.* **1998**, *54*, 139.
(21) Nguyen, T. C.; Ward, D. W.; Townes, J. A.; White, A. K.; Krantzman, K. D.; Garrison, B. J. *J. Phys. Chem. B* **2000**, *104*, 8221.
(22) Haberland, H.; Insepov, Z.; Moseler, M. *Phys. Rev. B* **1995**, *51*, 11061.
(23) Kerford, M.; Webb, R. P. *Nucl. Instrum. Methods Phys. Res., Sect. B* **2001**, *180*, 44.
(24) Colla, T. J.; Urbassek, H. M. *Nucl. Instrum. Methods Phys. Res., Sect. B* **2000**, *164*, 687.
(25) Webb, R.; Kerford, M.; Ali, E.; Dunn, M.; Knowles, L.; Lee, K.; Mistry, J.; Whitefoot, F. *Surf. Interface Anal.* **2001**, *31*, 297.
(26) Postawa, Z.; Czerwinski, B.; Szewczyk, M.; Smiley, E. J.; Winograd, N.; Garrison, B. J. *Anal. Chem.* **2003**, *75*, 4402.
(27) Postawa, Z.; Czerwinski, B.; Szewczyk, M.; Smiley, E. J.; Winograd, N.; Garrison, B. J. *J. Phys. Chem. B* **2004**, *108*, 7831.
(28) Postawa, Z.; Ludwig, K.; Piaskowy, J.; Krantzman, K.; Winograd, N.; Garrison, B. J. *Nucl. Instrum. Methods Phys. Res., Sect. B* **2003**, *202*, 168.
(29) Chatterjee, R.; Postawa, Z.; Winograd, N.; Garrison, B. J. *J. Phys. Chem. B* **1999**, *103*, 151.
(30) Meserole, C. A.; Vandeweert, E.; Postawa, Z.; Dou, Y.; Garrison, B. J.; Winograd, N. *Nucl. Instrum. Methods Phys. Res., Sect. B* **2001**, *180*, 53.
(31) Garrison, B. J. Molecular Dynamics Simulations, the Theoretical Partner to Static SIMS Experiments. In *ToF−SIMS: Surface Analysis by Mass Spectrometry*; Vickerman, J. C., Briggs, D., Eds.; Surface Spectra: Manchester, 2001; p 223.
(32) Garrison, B. J.; Delcorte, A.; Krantzman, K. D. *Acc. Chem. Res.* **2000**, *33*, 69.
(33) Garrison, B. J. *Chem. Soc. Rev.* **1992**, *21*, 155.
(34) Kelchner, C. L.; Halstead, D. M.; Perkins, L. S.; Wallace, N. M.; Depristo, A. E. *Surf. Sci.* **1994**, *310*, 425.
(35) Stuart, S. J.; Tutein, A. B.; Harrison, J. A. *J. Chem. Phys.* **2000**, *112*, 6472.
(36) Brenner, D. W. *Phys. Rev. B* **1990**, *42*, 9458.
(37) Brenner, D. W.; Harrison, J. A.; White, C. T.; Colton, R. J. *Thin Solid Films* **1991**, *206*, 220.
(38) Brenner, D. W.; Shenderova, O. A.; Harrison, J. A.; Stuart, S. J.; Ni, B.; Sinnott, S. B. *J. Phys.: Condens. Matter* **2002**, *14*, 783.
(39) Webb, R. P.; Kerford, M. *Nucl. Instrum. Methods Phys. Res., Sect. B* **2001**, *180*, 32.
(40) Adelman, S. A. D., J. D. *J. Chem. Phys.* **1974**, *61*, 4242.
(41) Garrison, B. J.; Kodali, P. B. S.; Srivastava, D. *Chem. Rev.* **1996**, *96*, 1327.
(42) Wucher, A.; Garrison, B. J. *Phys. Rev. B* **1992**, *46*, 4855.
(43) Wucher, A.; Garrison, B. J. *J. Chem. Phys.* **1996**, *105*, 5999.
(44) Delcorte, A.; Vanden Eynde, X.; Bertrand, P.; Vickerman, J. C.; Garrison, B. J. *J. Phys. Chem. B* **2000**, *104*, 2673.
(45) Kuhlewind, H.; Kiermeier, A.; Neusser, H. J. *J. Chem. Phys.* **1986**, *85*, 4427.
(46) Klippenstein, S. J.; Faulk, J. D.; Dunbar, R. C. *J. Chem. Phys.* **1993**, *98*, 243.
(47) Delcorte, A.; Bertrand, P.; Vickerman, J. C.; Garrison, B. J. How Do Large Organic Molecules Sputter? Insights from TOF−SIMS and Molecular Dynamics Simulations. In *Proceedings of the 12th International Conference on Secondary Ion Mass Spectrometry (SIMS XII)*; Benninghoven, A., Bertrand, P., Migeon, H.-N., Werner, H. W., Eds.; Elsevier: Amsterdam, 2000; p 27.
(48) Delcorte, A.; Garrison, B. J. *J. Phys. Chem. B* **2000**, *104*, 6785.
(49) Delcorte, A.; Garrison, B. J. *Nucl. Instrum. Methods Phys. Res., Sect. B* **2001**, *180*, 37.
(50) Garrison, B. J. *J. Am. Chem. Soc.* **1980**, *102*, 6553.
(51) Garrison, B. J. *J. Mass Spectrom.* **1983**, *53*, 243.
(52) Meserole, C. *Fundamental Studies of Energetic Ion Beam/Solid Surface Interactions*; Ph. D. Thesis, The Pennsylvania State University, 2002.
(53) Wojciechowski, I.; Sun, J. M.; Szakal, C.; Winograd, N.; Garrison, B. J. *J. Phys. Chem. A* **2004**, *108*, 2993.
(54) Wojciechowski, I. A.; Kutliev, U.; Sun, S. X.; Szakal, C.; Winograd, N.; Garrison, B. J. *Appl. Surf. Sci.* **2004**, *231−2*, 72.
(55) Wojciechowski, I., unpublished **2004**.
(56) **WEO 1**. Animation of Ga bombardment of the three layer of benzene on Ag system. A slice 1.5 nm wide in the center of the system is shown.
(57) **WEO 2**. Animation of C_{60} bombardment of the three layer of benzene on Ag system. A slice 1.5 nm wide in the center of the system is shown.